Preliminary aeroelastic design framework for composite wings subjected to gust loads

Rajpal, Darwin; De Breuker, Roeland

Publication date
2017

Published in
International Forum on Aeroelasticity and Structural Dynamics

Citation (APA)
Rajpal, D., & De Breuker, R. (2017). Preliminary aeroelastic design framework for composite wings subjected to gust loads. In *International Forum on Aeroelasticity and Structural Dynamics: IFASD 2017, 25-28 June 2017 Como, Italy*

International Forum on Aeroelasticity and Structural Dynamics
IFASD 2017
25-28 June 2017 Como, Italy

PRELIMINARY AEROELASTIC DESIGN FRAMEWORK FOR COMPOSITE WINGS SUBJECTED TO GUST LOADS

Darwin Rajpal[1] **and Roeland De Breuker**[1]

[1] Faculty of Aerospace Engineering
Delft University of Technology
Kluywerg 1, 2629 HS, Delft, The Netherlands
d.rajpal@tudelft.nl

Keywords: Gust loads, Structural Dynamics, Aeroelasticity, Optimization, Reduced Oder Model.

Abstract: Including a gust analysis in an optimization framework is computationally inefficient as the critical load cases are not known a priori and hence a large number of points within the flight envelope have to be analyzed. Model order reduction techniques can provide significant improvement in computational efficiency of an aeroelastic analysis. In this paper a reduced order aeroelastic model is formulated by reducing the aerodynamic system with a balanced proper orthogonal decomposition and coupling it to a structural solver. It is demonstrated that the dominant modes of the aerodynamic model can be assumed to be constant for varying equivalent airspeed and Mach number, enabling the use of a single reduced model for the entire flight envelope. Comparison of the results from the full and reduced order aeroelastic model shows a high accuracy of the latter and a large saving in computational cost. A dynamic aeroelastic optimization framework is then formulated using the reduced order aeroelastic model. Results show that both dynamic and static loads play a role in optimization of the wing structure. Furthermore, the worst case gust loads change during the optimization process and hence it is important to identify the critical loads at every iteration in the optimization.

1. INTRODUCTION

The goals set out by the European Commission in the Flightpath 2050 report [1], include, among others, a 75% reduction in CO_2 emissions per passenger kilometer, 90% reduction in NOx and 60% reduction in perceived noise by 2050 as compared to the aircraft in year 2000. These objectives do not seem to be realistic for conventional designs as it is becoming increasingly difficult to extract more performance out of the well-known wing and tube configuration. Advanced technologies such as composite materials and aeroelastic tailoring along with novel design seem to have the potential to address the required leap in performance. In the traditional design process, knowledge about the design increases, while the design freedom decreases, as we go from conceptual to preliminary and finally to the detailed design as shown in figure 1. For conventional designs, the lack of knowledge during the initial stages is compensated through empirical knowledge. However, lack of such empirical knowledge for a novel design, results in the need for increased physics based knowledge during the initial design process.

In the case of a conventional aircraft wing, during the early stages, based on the empirical knowledge, static load cases due to manoeuvres are considered as the most critical loads that

the aircraft will encounter. However, with the introduction of tailored composite materials, unsteady loads due to gusts can also become critical and hence the need to include them in the initial design process. In this paper, the focus is to incorporate the effect of the dynamic gust loads, in the preliminary structural design of the composite wings.

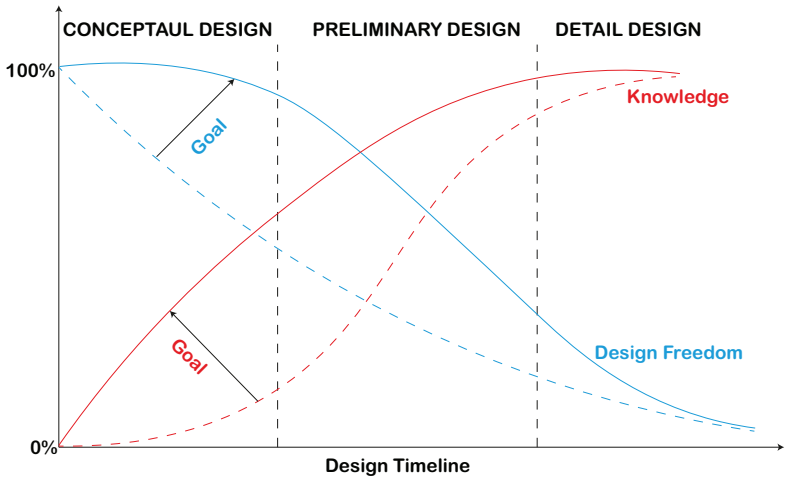

Figure 1: Trend of knowledge and freedom in aircraft design process [2]

Including the gust loads in an efficient and a reliable way during the initial phases of the design process is quite difficult. The first challenge is that there is no prior information on the flight point which will be critical with respect to dynamic loads. As per the requirements defined by the European Aviation Safety Agency (EASA) in the Certification Specifications for Large Aeroplanes (CS-25), a range of load cases across the entire flight envelope has to be taken into consideration to determine the maximum loads the aircraft structure will experience. A ball park approximation of the number of load cases to be taken into account can be in the order of 10 million [3]. This makes the process of finding the worst case gust loads computationally expensive. The second challenge is that as the design changes, the critical gusts might change as well and hence for every new iteration in the design process, the load cases have to be updated. This makes the inclusion of gust loads in the initial design process unfeasible. Thus the need for an efficient and robust way to compute unsteady loads.

The idea of improving the efficiency of the dynamic analysis has already received attention in recent years. Zeiler [4] used the concept of matched filter from signal processing to identify worst case stochastic gust loads. Fidkowski [5] also applied matched filter theory in combination with Lyapunov equation to identify critical load for the stochastic gust in the conceptual aircraft design process. Knoblach [6] used robust performance analysis from control theory to identify critical loads due to discrete 1-cosine gusts. In the work done under the European FP7 project FFAST [3, 7], surrogate modeling and optimization techniques were used for fast prediction of gust loads. Recently, Castellani et al. [8] applied model order reduction (MOR) technique to the aeroelastic system for rapid prediction of dynamic gust loads. The goal of the MOR techniques is to produce a system that shows similar response characteristics as the original, but consists of significantly fewer state variables, leading to reduction in computational cost. For determination of critical loads, Castellani et al. created a reduced aeroelastic model at different flight points and used interpolation techniques to cover the entire flight envelope.

In the present paper, the MOR has been applied to the aeroelastic system for calculation of various aircraft responses when subjected to discrete gust. A reduced order aeroelastic model

(ROAM) is formulated, based on a global reduced aerodynamic basis, independent of equivalent airspeed and free stream Mach number. The advantage of such an approach is that the reduced basis needs to be calculated only once and thus the need for interpolation is avoided. This makes the determination of critical gust loads computationally efficient. The accuracy of the formulated ROAM is demonstrated by comparing the results with the responses from the full-order model (FOM). Furthermore, an optimization framework is formulated using the ROAM which accounts for worst case gust loads at every iteration. To demonstrate the efficacy of such a framework, aeroelastic tailoring of the NASA Common Research Model (CRM) wing is carried out.

2. REDUCED ORDER AEROELASTIC MODEL

ROAM is based on the framework of PROTEUS, in-house aeroelastic tool, developed at the Delft University of Technology. In PROTEUS, the linear dynamic aeroelastic analysis is carried out around the non-linear static equilibrium solution. The non-linear structural stiffness matrix, obtained from the static analysis, is linearized and coupled to a linear mass matrix to obtain the dynamic structural model. This model is then coupled to an unsteady aerodynamic model based on the unsteady vortex lattice method. Using this linear dynamic analysis, the response of a wing to a discrete gust can be obtained. A detailed description of the PROTEUS is given in work by Werter and De Breuker [9]. In the following subsections, the formulation of ROAM has been described.

2.1. Aerodynamic model

In PROTEUS the aerodynamic model is based on the potential flow over a three-dimensional wing described by the Laplace equation, which is solved using the boundary element method (BEM). The wing is modeled as a thin wing with a prescribed wake using quadrilateral vortex rings with the collocation points in the center of the panels. Using the Kutta condition and Helmholtz theorem, a complete system of equations for the potential flow is given by

$$\mathbf{A}\boldsymbol{\Gamma}^t = -\mathbf{V}_\infty \cdot \mathbf{n} \tag{1}$$

$$\boldsymbol{\Gamma}^t_{TE} = \boldsymbol{\Gamma}^t_{w_0} \tag{2}$$

$$\mathbf{H}_1\boldsymbol{\Gamma}^t = \mathbf{H}_2\boldsymbol{\Gamma}^{t-1} \tag{3}$$

where the matrix $\mathbf{A}$ contains the aerodynamic influence coefficients, $\boldsymbol{\Gamma}$ is the vector of unknown vortex ring strengths, $\boldsymbol{\Gamma}_{TE}$ is the vector of unknown vortex ring strengths at the trailing edge of the wing, $\boldsymbol{\Gamma}_{w_0}$ is the vector of unknown vortex ring strengths at the start of the wake, and matrices $\mathbf{H}_1$ and $\mathbf{H}_2$ describe the transport of vorticity in the wake.

The vector with vortex ring strengths $\boldsymbol{\Gamma}$ can be split into three separate sets of unknowns: the body, Kutta, and wake unknowns. Using this separation of unknowns, the system of equations can be rewritten into the form of the standard state equation of a state-space system:

$$\dot{\mathbf{x}}_a = \mathbf{A}_a\mathbf{x}_a + \mathbf{B}_a\mathbf{u}, \tag{4}$$

where $\mathbf{A}_a$ is the state matrix, $\mathbf{B}_a$ is the input matrix, $\mathbf{u}$ is the input vector containing the time derivative of the angle of attack per spanwise section of the wing, and $\mathbf{x}_a$ is the state vector

containing the vortex strengths in the wake and angles of attack. The dot over the $\mathbf{x}$ indicates the time derivative. Combining equation (4) with expressions for the unsteady lift and moment acting on the wing, state-space system can be formulated as

$$\dot{\mathbf{x}}_a = \mathbf{A}_a\mathbf{x}_a + \mathbf{B}_a\mathbf{u}, \tag{5}$$

$$\mathbf{y}_a = \mathbf{C}_a\mathbf{x}_a + \mathbf{D}_a\mathbf{u}, \tag{6}$$

where $\mathbf{y}_a$ is the output vector containing the forces and moments acting on the wing per spanwise section. A more elaborate description of the aerodynamic modelling can be found in the work of Werter et al. [10].

The number of states in the vector $\mathbf{x}_a$ in state space system defined in equation 5 and 6 is in the order of $10^3 \sim 10^4$ thus leading to higher computational cost. By applying MOR methods, the dimension of the state vector $\mathbf{x}_a$ can be reduced, leading to increased computational efficiency. To develop a reduced aerodynamic system, the original states of the linear time-invariant (LTI) state-space system is projected onto a reduced basis:

$$\mathbf{x}_a = \mathbf{V}_r\mathbf{c}, \tag{7}$$

where $\mathbf{c}$ is a vector with the r reduced states and $\mathbf{V}_r$ is the reduced basis onto which the original states are projected. Inserting this equation into equations (5) and (6), results in

$$\dot{\mathbf{c}} = \mathbf{V}_r^{-1}\mathbf{A}_a\mathbf{V}_r\mathbf{c} + \mathbf{V}_r^{-1}\mathbf{B}_a\mathbf{u} = \mathbf{A}_r\mathbf{c} + \mathbf{B}_r\mathbf{u}, \tag{8}$$

$$\mathbf{y}_a = \mathbf{C}_a\mathbf{V}_r\mathbf{c} + \mathbf{D}_a\mathbf{u} = \mathbf{C}_r\mathbf{c} + \mathbf{D}_a\mathbf{u}. \tag{9}$$

The number of states r in the ROAM depends on the required accuracy and the basis $\mathbf{V}_r$, but is typically in the order of $10 \sim 100$. There are four different MOR methods that are often used to provide the reduced basis. The methods are modal truncation (MT), balanced truncation (BT), proper orthogonal decomposition (POD) and balanced proper orthogonal decomposition (BPOD). In a previous study performed by Gillebaart and De Breuker [11], four MOR methods were applied to a continuous-time state-space unsteady aerodynamic model and their specific properties, accuracy, robustness, and computational efficiency were investigated. The BPOD method provided the best combination of high accuracy with very few states, relatively low computational cost for a typical model size of interest, and sufficient robustness. Consequently in the current study BPOD method was chosen to compute the reduced basis for the aerodynamic system.

For determination of critical loads, the aeroelastic system must be solved over a large number of flight points to calculate the various responses of the aircraft over the entire flight envelope. A significant saving in computational expense can be achieved if a reduced-order aeroelastic system can be used instead of a full order system. However, the full order aerodynamic system depends on parameters such as altitude, Mach number and velocity, hence every new flight point would necessitate a new ROAM. Thus an efficient way of applying the reduced order aeroelastic system without the need of performing a new reduction at each flight point has been formulated.

Benner et al. [12] have provided a comprehensive survey on MOR for a parametric state space system. Generally, the approaches for the parametric model order reduction can be differentiated into local and global based methods. In the local based methods [13, 14], the reduced basis required at a given point can be generated by interpolating local reduced bases generated

at fixed number of points in the parameter space . In the global based methods [15], a single reduced basis is generated by projecting the global matrix containing snapshots at various points in the parameter space. By projecting a global matrix, dominant modes across entire parameter space are selected, thus giving a good approximation. For the current aerodynamic system, a method similar to the global based methods is used. A reasonable assumption can be made that, for a given wing planform, the dominant modes will be the same for all the points inside the flight envelope. The basis for this assumption is explained below.

For every point inside the flight envelope, the aerodynamic state space matrices depend upon the equivalent air speed (V_{EAS}), and the free stream Mach number, M. For the assumption to be valid, the dominant modes of the system should not change with a change in V_{EAS} and M. With respect to V_{EAS}, taking a look at the aerodynamic system of equations described in equations 1, 2 and 3, the effect of velocity is included in the right hand side of equation 1. The aerodynamic influence coefficient (AIC) matrix in equation 1 also depends upon the velocity. A change in velocity necessitates a change in the trim angle, which leads to a change in the geometry of the mesh. However, in a linear analysis, for small deviations in the trim angle, the AIC matrix can be assumed to be constant. Thus the aerodynamic system can be assumed to have an affine dependency on the velocity. The aerodynamic state space system described in equation 5 and 6 can then be formulated as

$$\dot{\mathbf{x}}_a = \mathbf{F}_1(V_{eq})\hat{\mathbf{A}}_\mathbf{a}\mathbf{x}_a + \mathbf{F}_2(V_{eq})\hat{\mathbf{B}}_a\mathbf{u}, \tag{10}$$

$$\mathbf{y}_a = \mathbf{F}_3(V_{eq})\hat{\mathbf{C}}_a\mathbf{x}_a + \mathbf{F}_4(V_{eq})\hat{\mathbf{D}}_a\mathbf{u}, \tag{11}$$

where the modified state-space matrices are now independent of the equivalent airspeed, and the influence of the airspeed is collected in the matrices $\mathbf{F}_1$ to $\mathbf{F}_4$. These matrices are found by taking out the dependencies of the equivalent airspeed during the formulation of the state-space system. As a result, the characteristics of the state matrix will remain the same for different velocities, validating the assumption that dominant modes for different velocities can be assumed to be the same.

Before describing the effect of Mach number on the mode shapes, the effect of change in aspect ratio on the mode shapes is investigated. In Figure 2 the mode shapes for the backward swept wing are shown for the 4 different aspect ratios of the wing. The aspect ratios are 9.5, 8, 6.5 and 5. Please note that only the shapes along the chordwise and spanwise directions with the origin at the root trailing edge point are displayed to enable a good comparison between the mode shapes for different aspect ratios.

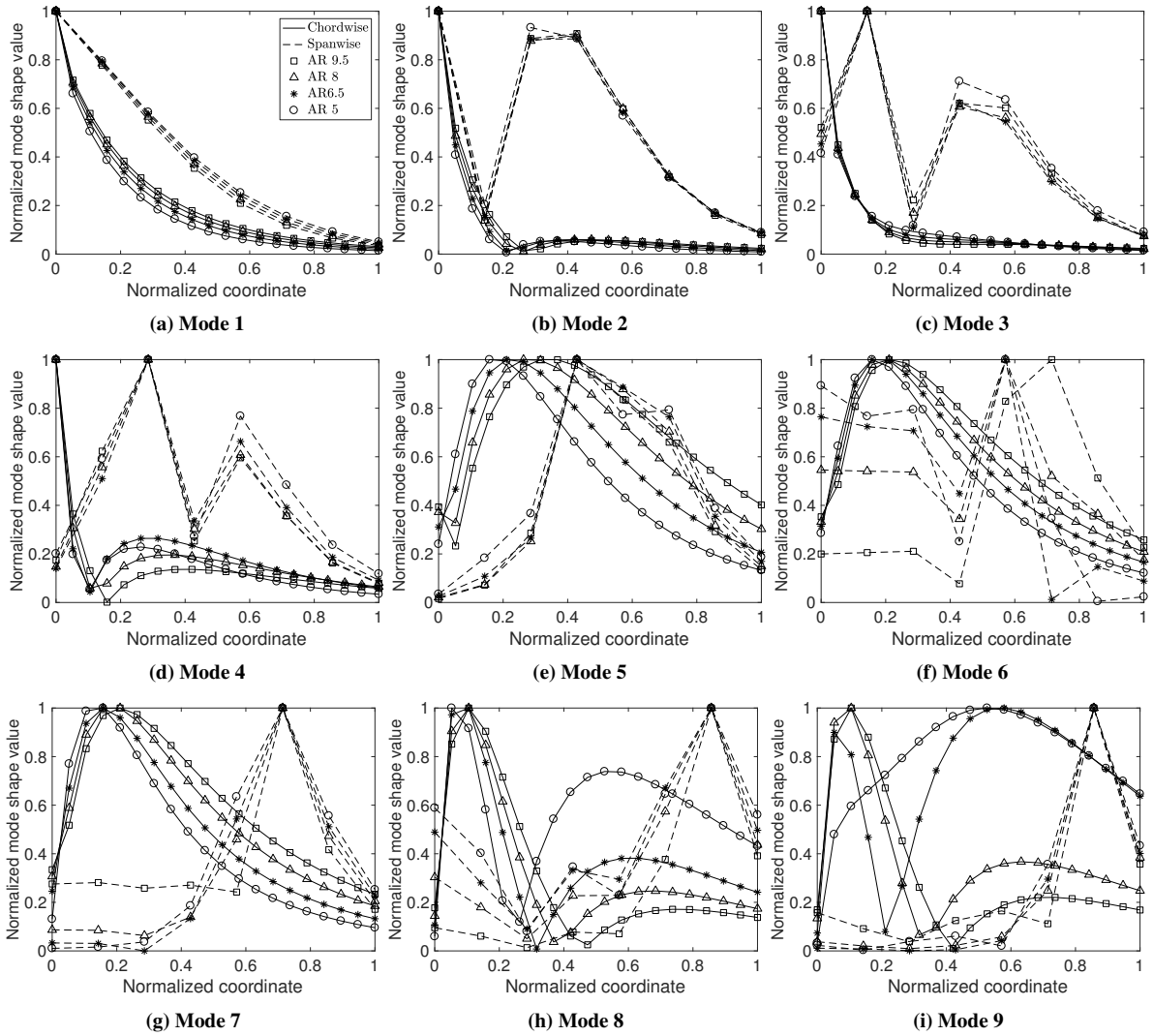

(a) Mode 1 **(b) Mode 2** **(c) Mode 3**

(d) Mode 4 **(e) Mode 5** **(f) Mode 6**

(g) Mode 7 **(h) Mode 8** **(i) Mode 9**

Figure 2: First 9 BPOD mode shapes for a untapered, swept backward wing for different aspect ratios.

The mode shapes for the first three, most dominant modes, are practically constant with changing aspect ratio of the wing. Up to mode 7 the shapes remain very similar. As the mode number increases further, a larger difference is seen with increasing aspect ratio, although the trend is still similar. A conclusion can be made that mode shapes for the first 7 dominant modes remain almost similar for different aspect ratio.

With respect to the Mach number effects, the application of Prandtl Glauert transformation brings the parametric dependency of the aerodynamic system on the Mach number. The Prandtl Glauert transformation scales the geometry in the x-direction by factor $\sqrt{1-M^2}$, effectively changing the aspect ratio of the wing. The first seven dominant modes of the aerodynamic system stay nearly constant with the change in the aspect ratio. Hence, a change in Mach number results in a nearly no change in the dominant modes. Thus, with the assumptions mentioned before, a reduced basis constructed at one flight point can reasonably span the entire flight envelope.

2.2. Aeroelastic Framework

In the present work, the reduced order aerodynamic system, as described in the previous section, generated using BPOD, replaces the full order unsteady aerodynamic model in the PROTEUS framework . For the purpose of completeness, the state space equation for the coupled dynamic system is derived. The governing equation of a linear dynamic structural model is given by:

$$\mathbf{M}\ddot{\mathbf{p}} + \mathbf{K}\mathbf{p} = \mathbf{F}_s \tag{12}$$

where $\mathbf{M}$ is the global mass matrix, $\mathbf{K}$ is the global stiffness matrix, $\mathbf{p}$ contains the structural degrees of freedom and $\mathbf{F}_s$ is the force vector. This system of equations can be converted to a first order state-space system by including both $\dot{\mathbf{p}}$ and $\mathbf{p}$ in the vector of state variables, resulting in:

$$\begin{pmatrix}\ddot{\mathbf{p}}\\ \dot{\mathbf{p}}\end{pmatrix} = \begin{bmatrix}\mathbf{0} & -\mathbf{M}^{-1}\mathbf{K}\\ \mathbf{I} & \mathbf{0}\end{bmatrix}\begin{pmatrix}\dot{\mathbf{p}}\\ \mathbf{p}\end{pmatrix} + \begin{bmatrix}\mathbf{M}^{-1}\\ \mathbf{0}\end{bmatrix}\begin{pmatrix}\mathbf{F}_s\\ \mathbf{0}\end{pmatrix} \tag{13}$$

$$\begin{pmatrix}\ddot{\mathbf{p}}\\ \dot{\mathbf{p}}\end{pmatrix} = \mathbf{A}_s\begin{pmatrix}\dot{\mathbf{p}}\\ \mathbf{p}\end{pmatrix} + \mathbf{B}_s\begin{pmatrix}\mathbf{F}_s\\ \mathbf{0}\end{pmatrix} \tag{14}$$

where $\mathbf{I}$ is the identity matrix, $\mathbf{0}$ the zero matrix, and $\mathbf{A}_s$ and $\mathbf{B}_s$ the structural state and input matrices, respectively. Coupling equations 8, 9 and 14 and performing some algebraic manipulation, results in the reduced-order dynamic aeroelastic state space system:

$$\dot{\mathbf{x}} = \mathbf{A}_{ae}\mathbf{x} + \mathbf{B}_{ae}\mathbf{u} \tag{15}$$

$$\begin{pmatrix}\mathbf{F}\\ \mathbf{p}\end{pmatrix} = \mathbf{C}_{ae}\mathbf{x} + \mathbf{D}_{ae}\mathbf{u} \tag{16}$$

where the state vector $\mathbf{x}$ is given by $\begin{bmatrix}\mathbf{c} & \dot{\mathbf{p}} & \mathbf{p}\end{bmatrix}^T$, $\mathbf{F}$ contains unsteady lift and moment forces and $\mathbf{A}_{ae}$, $\mathbf{B}_{ae}$, $\mathbf{C}_{ae}$ and $\mathbf{D}_{ae}$ are the aeroelastic state, input, output and feedthrough matrices.

2.3. Common Research Model

The NASA CRM [16], originally developed for the 4th AIAA drag prediction workshop, is used as a case study for the current analysis. The aircraft main characteristics are summarized in Table 1. Figure 3 depicts the wing planform. The wing consist of 54 ribs with a rib spacing of 0.55 m that are taken into account as concentrated masses. Additionally engine, leading edge devices and trailing edge devices are also accounted for as concentrated masses. The top and bottom skin of the wing is strengthened with the help of stringers that run along the span of the wing.

Parameter	Value
Span	58.769 m
Leading edge sweep angle	35 deg
Wing aspect ratio	8.4
Taper ratio	0.275
Planform wing area	412 m^2
Cruise Mach	0.85
Design Range	14,300 km
Design Payload	45,000 kg
Fuel Weight	105,000 kg
Operational empty weight	146,100 kg
Maximum takeoff weight	296,000 kg

Table 1: Characteristics of the CRM wing.

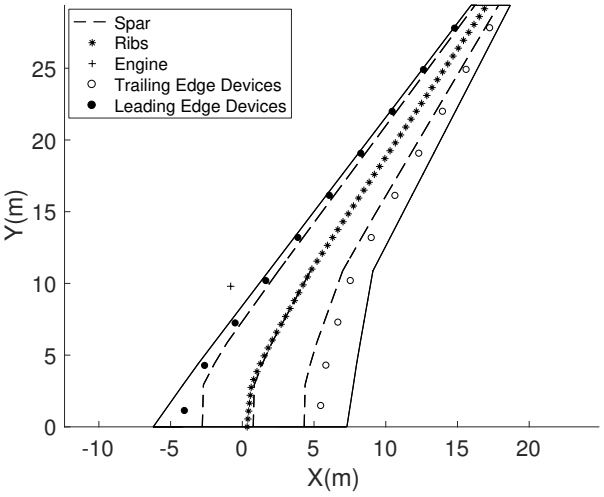

Figure 3: CRM wing planform.

2.4. Response to Varying Gust Length

To demonstrate the application of the reduced-order aeroelastic framework in determining the gust response of aircraft, the CRM wing model is subjected to a discrete 1-cosine gust of varying gust lengths. The 1-cosine profile for the discrete gust is given by [17]

$$U = \frac{U_{ds}}{2}\left(1 - \cos\left(\frac{\pi s}{H}\right)\right) \tag{17}$$

where U is the gust velocity, s the distance penetrated into the gust, H the gust gradient, and U_{ds} the design gust velocity defined as

$$U_{ds} = U_{ref} F_g \left(\frac{H}{350}\right)^{1/6} \tag{18}$$

where U_{ref} is the reference velocity that reduces bi-linearly from 17.07 m/s at sea level to 13.41 m/s at 4,572 m and then to 6.36 m/s at 18,288 m, and F_g is the flight profile alleviation factor related to the aircraft maximum take-off weight and maximum landing weight.

Figure 4 depicts the four different gust velocity profile having gust gradients of 9 m, 30 m, 80 m and 110 m. Figures 5 and 6 depict the root bending moment and root torsional moment responses of the CRM wing to the four different gust gradients as obtained by the FOM and the ROAM, using 20 out of 1188 modes, for a flight point of $M = 0.73$ at an altitude of 11,000 m. As can be seen, the responses from the ROAM give a good accuracy as compared to the responses from the FOM with the error being less than 0.5% across the entire time history. With respect to efficiency, the ROAM took 160 s to build and 1.2 s to simulate whereas the FOM took 29.3 s to simulate. The time required for building the ROAM outweighs the benefit in this case, because only a small number of flight points are included. The simulation time, however, is decreased by 96%, so if more flight points will be included the reduction in simulation time will at some point outweigh the time spend on building the ROAM, as is demonstrated in the next subsection.

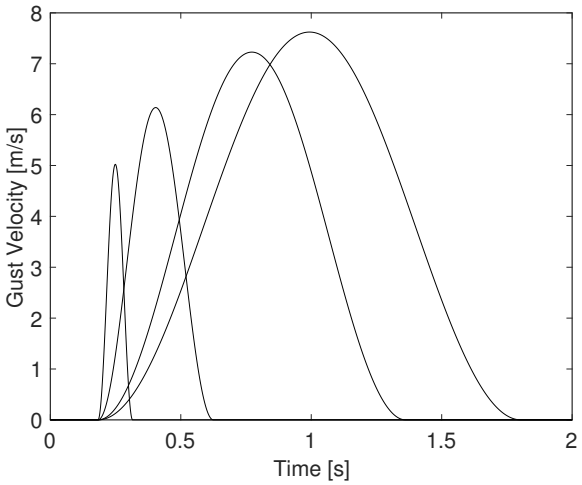

Figure 4: Gust Profile for different gust gradients

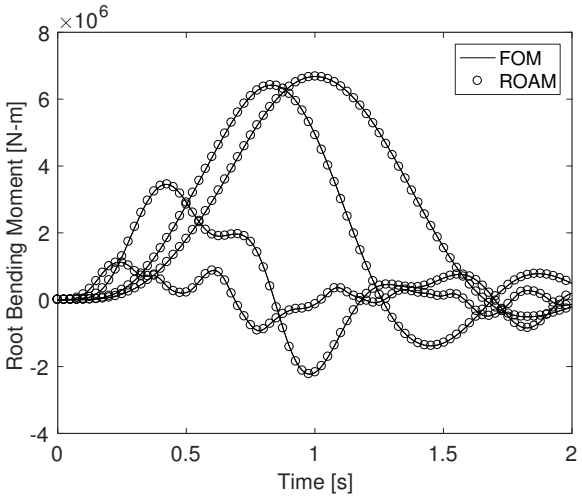

Figure 5: Root bending moment response for the FOM and ROAM of the CRM wing.

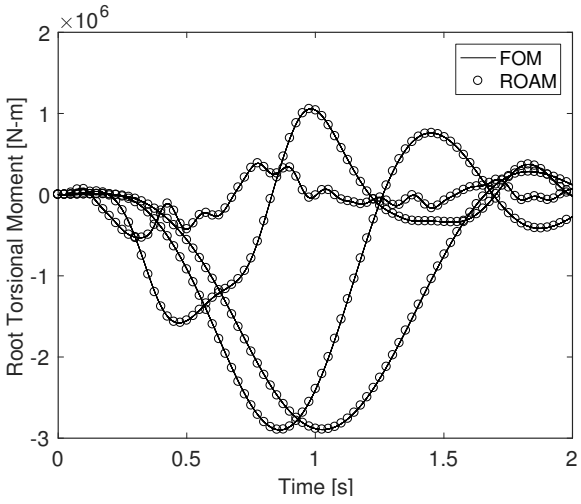

Figure 6: Root torsional moment response for the FOM and ROAM of the CRM wing.

2.5. Response across the flight envelope

To demonstrate the applicability of the reduction method, the response of the standard backward swept CRM wing and a forward swept version of the CRM wing using both the ROAM and the FOM is evaluated at 36 different flight points across the flight envelope. For each flight point, 68 different gust gradients, ranging from 9 m to 107 m, are considered, bringing the total number of evaluated flight points to 2448. Table 2 gives a summary of the different flight condition considered in this study. A reduced basis is calculated at the cruise condition with a cruise speed of 220 m/s at 10 km altitude and a Mach number of 0.73. The altitude has been reduced from the standard 11 km to 10 km in order to bring down the Mach number and remain within the validity of the potential flow theory. The first 20 out of a total of 1188 aerodynamic modes of this basis are used as the global reduced basis for the ROAM.

Flight parameter	Number
Flight speed	3
Altitude	12
Gust gradient	68
Total number of points	2,448

Table 2: List of flight points

The load plots over the complete flight envelope, also called potato plots, for combination of root bending moment, root shear force and root torsional moment for both backward swept wing and forward swept wing are shown in figures 7, 8, 9 and 10. A good agreement of the ROAM with the FOM across the entire flight envelope is obtained with the error being less than 0.5%.

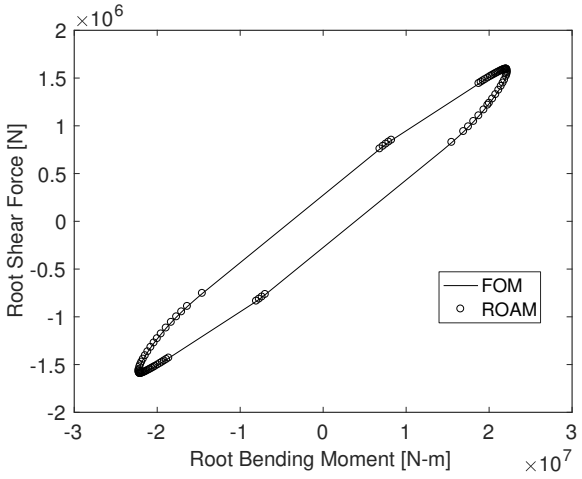

Figure 7: Root bending moment versus shear force for the backward swept CRM.

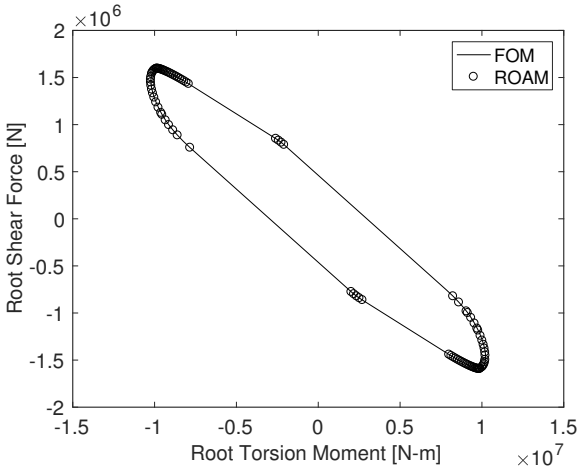

Figure 8: Root torsion moment versus shear force for the backward swept CRM.

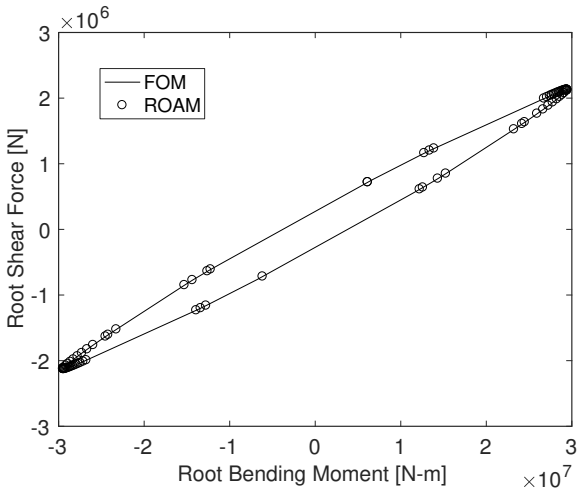

Figure 9: Root bending moment versus shear force for the forward swept CRM.

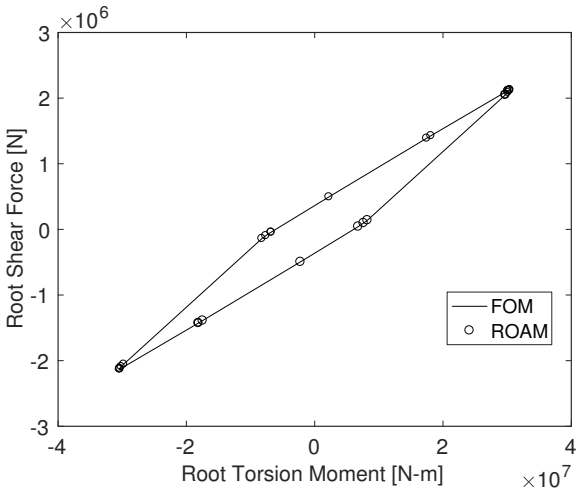

Figure 10: Root torsion moment versus shear force for the forward swept CRM.

Table 3 compares the computational effort required by the FOM and the ROAM for sweeping

the flight envelope. The time related to the model setup for the ROAM is kept low by using the single reduced basis as the global basis, as was explained before. The achieved reduction in simulation time is an order of magnitude larger than the extra time required for creating the ROAM, resulting in an 85.5% saving in the computational effort in identifying the critical loads.

	Model setup (min)	**Simulation time** (min)	**Total time** (min)
FOM	0	171	171
ROAM	2.7	22.1	24.8
Difference	2.7 (-)	148.9 (87.1%)	146.2 (85.5%)

Table 3: Breakdown of computational time required for the critical load identification

3. OPTIMIZATION FRAMEWORK

As has been mentioned before, in the case of gust loads, there is no prior information on the flight point which leads to the critical load. During the optimization process, for every iteration, an update in the design of the wing would lead to a modification in the aeroelastic characteristics of the wing, which could result in a different critical gust loads. As a result, at every iteration, range of load cases across the entire flight envelope needs to be evaluated to determine the worst case gust loads. Hence an optimization framework, depicted in figure 11, is formulated which has the capability to determine the critical gust load at every iteration in a computationally efficient manner. It starts with identification of the worst gust load for the initial design using the ROAM. Next, for the given critical dynamic and static load conditions, PROTEUS analyses the initial design and calculates the analytical sensitivities which are then fed to the optimizer. Optimizer calculates the new design variables which are fed to ROAM as well as PROTEUS. ROAM analyzes the entire flight envelope with respect to the new design variables, identifies the critical loads and feeds it back to PROTEUS. The process continues till the optimum has reached.

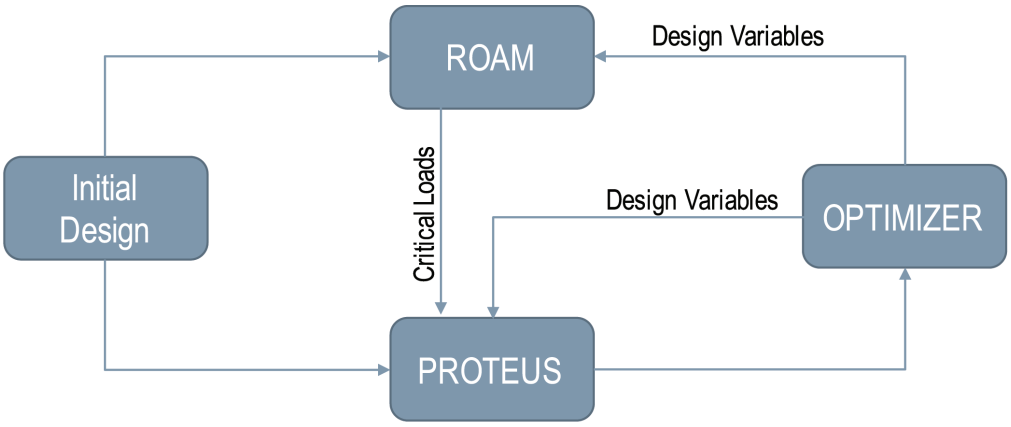

Figure 11: Schematic representation of the optimization framework

3.1. Optimization Setup

In order to assess the potential of the framework for aeroelastic tailoring of the wing and investigate the importance of the gust loads, stiffness and thickness optimization of the aforementioned CRM wing is carried out. Table 4 shows the material properties used for the CRM wing. To account for the effect of material scatter, barely visible impact damage and environmental effects, the strength allowables are knocked down by a factor of 0.416 [18]. Table 5 gives the information regarding the optimization setup considered in the current study. The objective is to minimize the structural weight of the wing. The wing is divided into 10 spanwise sections. Each section of the top skin and the bottom skin consists of two laminates in the chord-wise direction and each section of the spar has one laminate. This distribution results in 64 unique laminates. The laminates are represented by lamination parameters which describe the in-plane and out-of-plane behaviour of the composite laminates which are symmetric and unbalanced. For every laminate there are eight lamination parameters and one thickness variable resulting in a total number of 576 design variables. Figure 12 depicts the laminate distribution along the top skin of the wing. It also shows the stiffness for each laminate, where the wing stiffness distribution is represented by the polar plot of thickness normalized modulus of elasticity $\mathbf{E}_{11}(\theta)$ which is given by

$$\mathbf{E}_{11}(\theta) = \frac{1}{\mathbf{A}_{11}^{-1}(\theta)} \tag{19}$$

where $\mathbf{A}$ is the membrane stiffness matrix and θ ranges from 0 to 360 degrees.

Property	Value
E_{11}	147 GPa
E_{22}	10.3 GPa
G_{12}	7 GPa
ν_{12}	0.27 GPa
ρ	1600 kg/m^3
X_t	2280MPa
X_c	1725MPa
Y_t	57MPa
Y_c	228MPa
S	76MPa

Table 4: Material Properties

Type	Parameter	Number
Objective	Minimize Wing Mass	1
Design Variables	Lamination Parameter	576
	Laminate Thickness	
Constraints	Laminate Feasibility	384
	Static Strength	1024/loadcase
	Buckling	4096/loadcase
	Aeroelastic Stability	10/loadcase
	Aileron Effectiveness	1/loadcase
	Local Angle of Attack	22/loadcase

Table 5: Optimization Setup

Lamination feasibility equations formulated by Hammer et al. [19], Raju et al. [20] and Wu et al. [21] are applied to make sure that the lamination parameter represents the actual ply distribution. The static strength of the laminate is assessed by the failure envelope calculated using Tsai-Wu criterion formulated for lamination parameter domain by Khani et al. [22]. The stability of the panel in buckling is based on idealized buckling model formulated by Dillinger et al. [23]. To ensure that the wing is aeroelastically stable, the real part of the eigenvalues of the state matrix should be less than zero. The local angle of attack is constrained to a maximum of 12 degrees and a minimum of -12 degrees. The aileron effectiveness [23] computed as the negative ratio of the roll coefficient induced by the aileron deflection and the roll coefficient due to the roll manoeuvre is set to a minimum of 0.1 to ensure reasonable handling quality. For the current optimization, the Globally Convergent Method of Moving Asymptotes (GCMMA) developed by Svanberg [24] is used as a gradient-based optimizer.

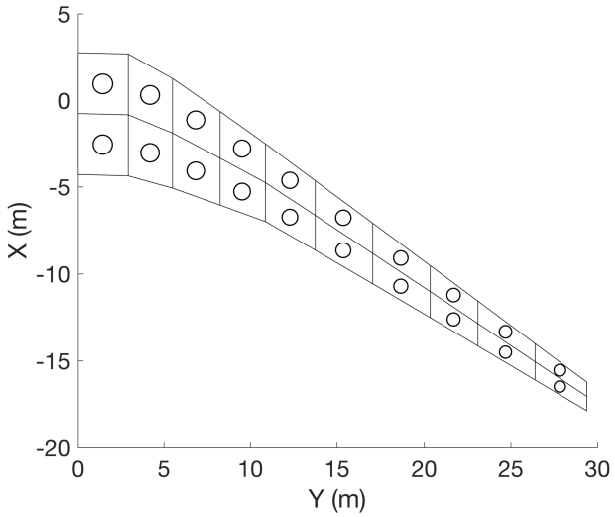

Figure 12: Laminate Distribution of the top skin of CRM

Table 6 gives the information on the static loadcases which are used for the current study. These loadcases which were provided by NASA, represents the cruise condition, 2.5g symmetric pull up manoeuvre and -1g symmetric pull down manoeuvre. With respect to dynamic loadcases, 84 flight points covering the entire flight envelope will be investigated to select the critical load case. For each flight point, 40 gust gradient both positive as well as negative, ranging from 9m to 107m will be investigated. Thus, in total 3360 load cases will be scanned to determine the critical loads. Figure 13 displays the flight envelope with their respective flight point ID.

Loadcase ID	$\mathbf{V_{EAS}}$ (m/s)	**Altitude** (m)	**Load Factor**	**Fuel level/Max fuel** (%)
1	136	11000	1	70
2	240	3000	2.5	80
3	198	0	-1	80

Table 6: List of Static Loadcases

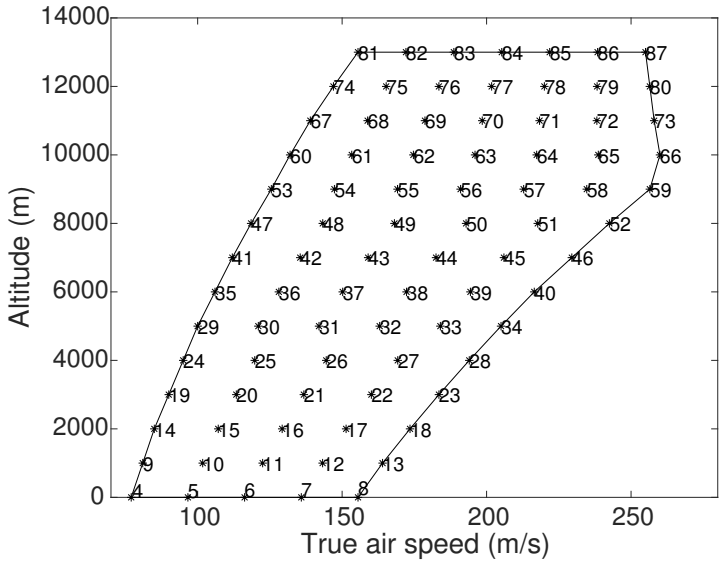

Figure 13: Flight Envelope

3.2. Results

3.2.1. Critical Gust load

Figure 14 and 15 depicts the critical loads at various iterations in the optimization process on the top and bottom skin of the CRM wing respectively. For each laminate, the number indicates the critical flight point and the colour indicates the critical gust gradient. Flight points 1, 2 and 3 are static load cases described in table 6 and the rest are the dynamic flight points as shown in the figure 13. Looking at the critical loads, the change in the design variables leads to modification in the aeroelastic properties of the wing, which results in variation of critical loads. Figure 16 shows the mean change in the design variables along the optimization process and figure 17 shows the corresponding change in the frequency of the first bending mode. Additionally, figure 18 shows for every iteration, the number of critical load cases that have been added or removed with respect to the previous iteration. As can be seen, the biggest change in the design variable as well as the mode frequency happens in the first few iterations. As a result, the change in the critical loads is also significant in the first few iterations. Thus, in the case of dynamic aeroelastic optimization process, the worst case gust loads need to be determined at every new iteration during the first few steps as the change in the later steps is minimal.

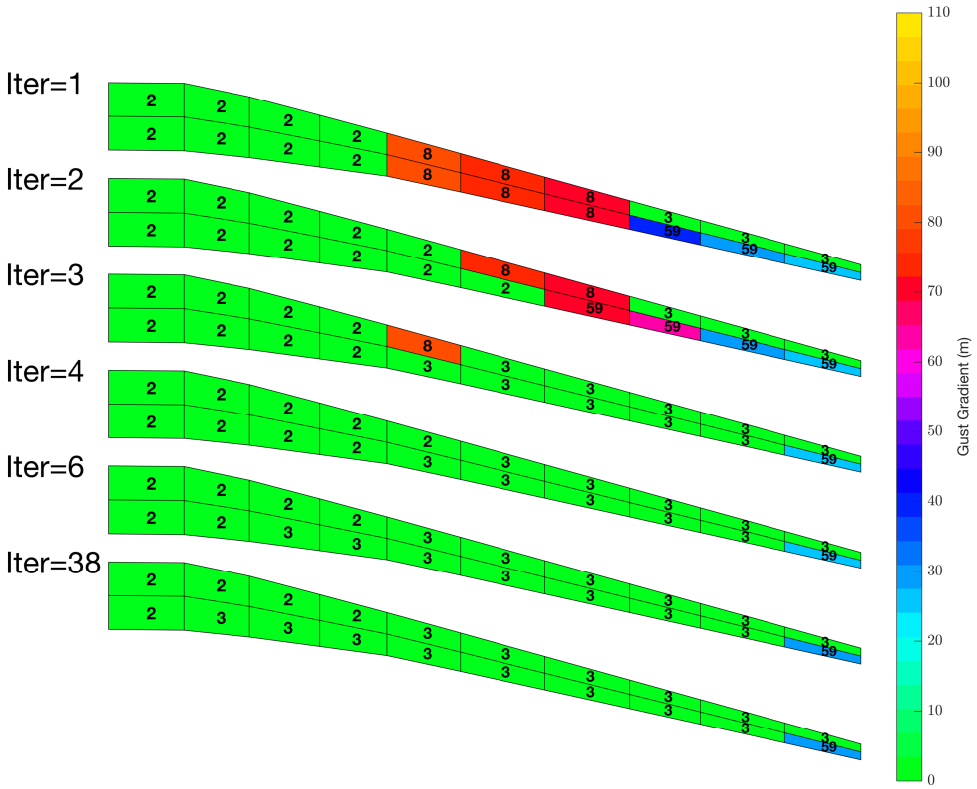

Figure 14: Critical flight points and gust gradients on the top skin during the optimization process

Looking at the flight points responsible for the worst case gust loads, one would have expected, the cruise condition to be the most critical flight point. However, gust response is dominated by the dynamic pressure and the reference gust velocity. As per the certification requirements, the reference gust velocity decreases as the altitude increases. Hence, along with cruise load case, the points at sea level also are responsible for the critical gust loads. With respect to gust gradient, critical length increases as we move from the outer part towards the inner part of the wing.

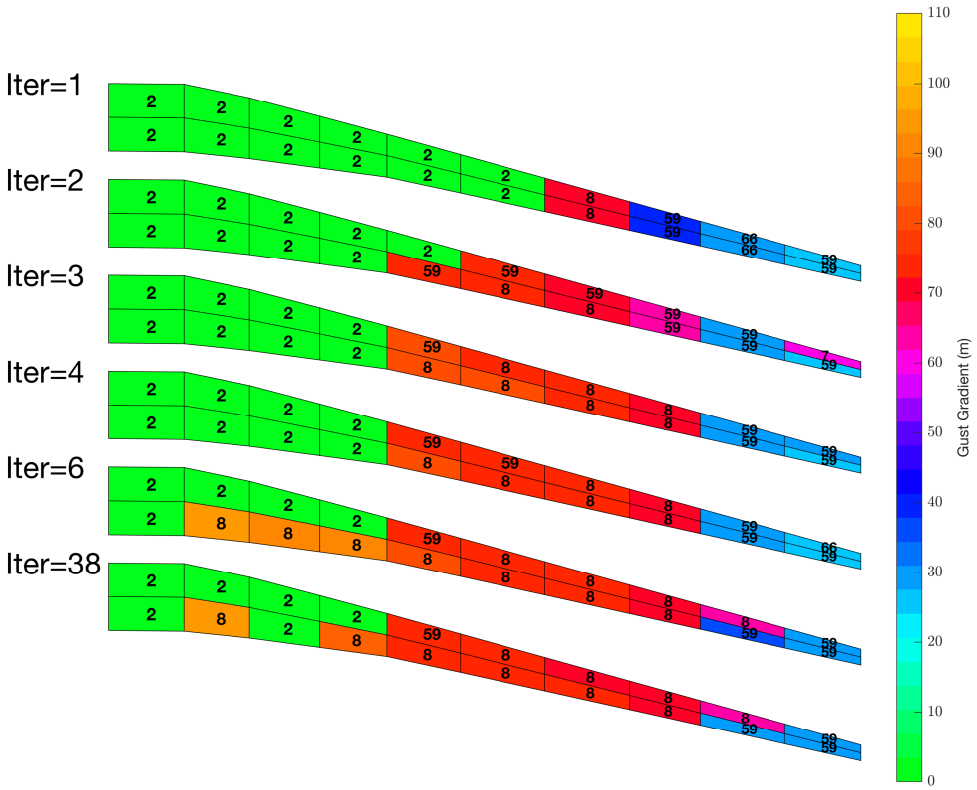

Figure 15: Critical flight points and gust gradients on the bottom skin during the optimization process

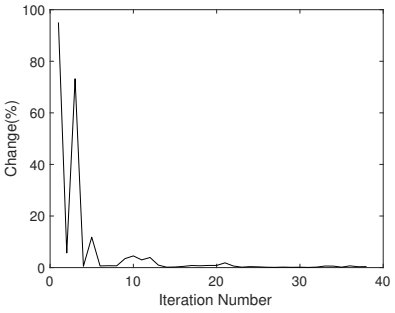

Figure 16: Mean change in the design variables

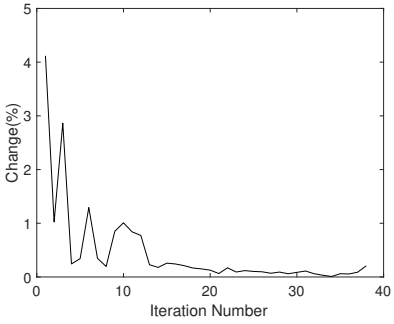

Figure 17: Change in the 1st bending frequency

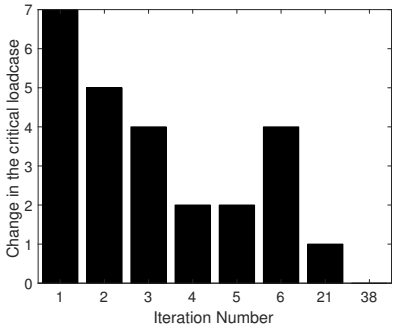

Figure 18: Total number of the change in the critical loadcases

3.2.2. Optimized Design

The structural weight of the optimized wing is 8,684 kg which is 86.5% of the initial weight. Figure 19 shows the stiffness and the thickness distribution of the optimized CRM wing. The strain, and buckling constraints can be seen in figure 20. The inner half of the wing is mainly dominated by strain and buckling constraints, whereas the outer half is dominated by aileron efficiency and strain constraints. In the inner half, the region near the wing root is dominated by buckling and as a result the out of plane stiffness properties are more pronounced as compared to the rest of the wing. The middle part of the wing is sized by the strain and hence the in-plane stiffness are oriented along the wing axis to maximize the load carrying capabilities of the wing. The thickness in the inner half of the wing increases from the root till the region around the engine. Additionally, the front part has a higher thickness as compared to the aft, thus shifting the elastic axis forward and introducing wash-out twist upon wing bending which alleviates the load. In the outer half of the wing the in-plane stiffness are oriented aft to increase the aileron effectiveness. Furthermore the aft part is thicker than front part, shifting the elastic axis aft thus making it beneficial in terms of aileron effectiveness.

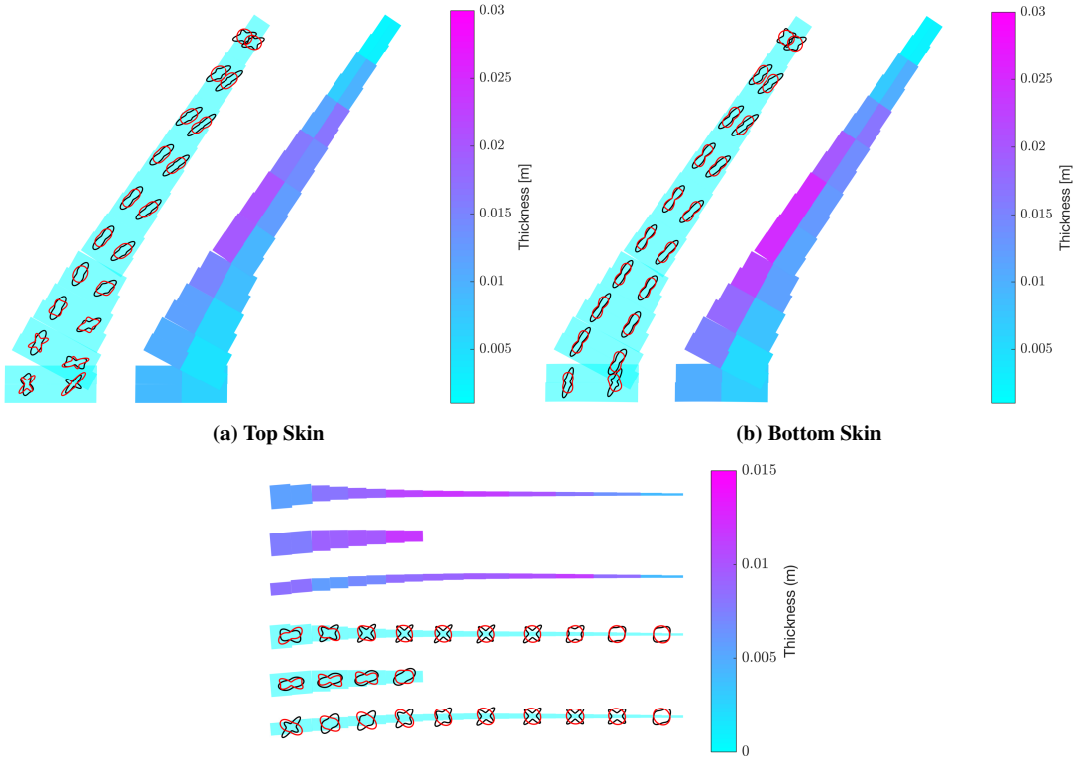

(a) Top Skin **(b) Bottom Skin**

(c) Spars

Figure 19: Stiffness and thickness distribution for the optimized CRM wing (In-plane stiffness: blue, out-of-plane stiffness: red.)

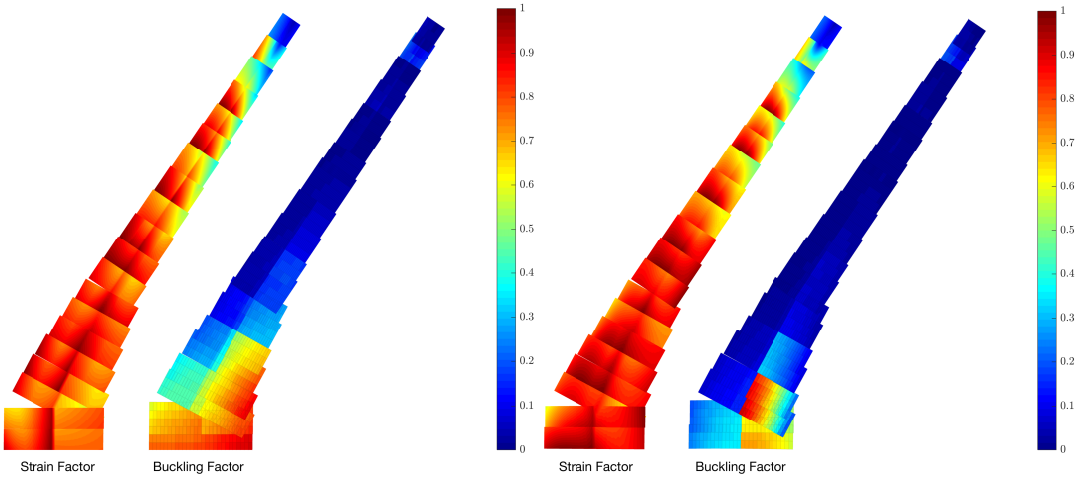

(a) Top Skin **(b) Bottom Skin**

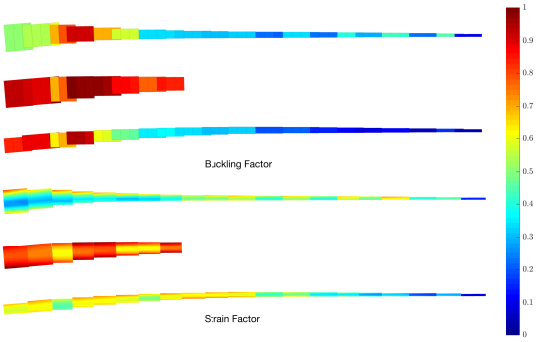

(c) Spars

Figure 20: Strain and buckling factor distribution on the optimized CRM wing.

4. CONCLUSIONS

In this paper, a ROAM was formulated using the BPOD method. It was shown that the ROAM predicts the wing responses caused by different gust gradients very accurately. To be able to efficiently cover the complete flight envelope of an aircraft for a given wing planform, a new formulation for the state-space system was derived where the influence of the equivalent airspeed was isolated from the state-space matrices. Furthermore, it was demonstrated that the Mach number, which in this vortex lattice method is implemented using the Prandtl-Glauert correction, has a negligible effect on the reduced basis. A single reduced-order model (ROM) could thus be used to analyze the aeroelastic loads throughout the flight envelope, reducing the computational cost significantly. The comparison of the loads acting on a backward and forward swept version of the NASA CRM obtained with the ROAM and FOM proved the validity of the assumption. A large saving in computational cost of 89% for the analysis of 2448 flight points was obtained using this method.

Using the developed ROAM, a dynamic aeroelastic optimization framework was formulated and thickness and stiffness optimization of the CRM wing was carried out. The results showed that the change in the design variables were highest during the first few iterations which lead to considerable change in the critical loads in the first few iterations. This showed the importance of identifying the critical loads at every iteration in the dynamic aeroelastic optimization process.

5. REFERENCES

[1] Krein, A. and Williams, G. (2012). Flightpath 2050: Europe's vision for aeronautics. *Innovation for Sustainable Aviation in a Global Environment: Proceedings of the Sixth European Aeronautics Days, Madrid, 30 March-1 April, 2011*, 63.

[2] Mavris, D. N. and DeLaurentis, D. A. (2000). Methodology for examining the simultaneous impact of requirements, vehicle characteristics, and technologies on military aircraft design.

[3] Khodaparast, H. H., Georgiou, G., Cooper, J. E., et al. (2012). Efficient worst case 1-cosine gust loads prediction. *Journal of Aeroelasticity and Structural Dynamics*, 2(3).

[4] Zeiler, T. A. (1997). Matched filter concept and maximum gust loads. *Journal of aircraft*, 34(1), 101–108.

[5] Fidkowski, K. J., Engelsen, F., Willcox, K. E., et al. (2008). Stochastic gust analysis techniques for aircraft conceptual design. In *12th AIAA/ISSMO Multidisciplinary Analysis and Optimization Conference*. p. 5848.

[6] Knoblach, A. (2013). Robust performance analysis applied to gust loads computation. *Journal of Aeroelasticity and Structural Dynamics*, 3(1).

[7] Khodaparast, H. H. and Cooper, J. E. (2013). Worst case gust loads prediction using surrogate models and system identification methods. In *Proceedings of 54th AIAA/ASME/ASCE/AHS/ASC Structures, Structural Dynamics and Materials Conference, Boston, MA*.

[8] Castellani, M., Lemmens, Y., and Cooper, J. E. (2015). Parametric reduced order model for rapid prediction of dynamic loads and aeroelastic response with structural nonlinearities. In *International Forum on Aeroelasticity and Structural Dynamics, St. Petersburg, Russia*.

[9] Werter, N. P. M. and De Breuker, R. (2016). A novel dynamic aeroelastic framework for aeroelastic tailoring and structural optimisation. *Composite Structures*, 158, 369–386. ISSN 0263-8223. doi:10.1016/j.compstruct.2016.09.044.

[10] Werter, N. P. M., De Breuker, R., and Abdalla, M. M. (2015). Continuous-time state-space unsteady aerodynamic modelling for efficient aeroelastic load analysis. In *International Forum on Aeroelasticity and Structural Dynamics, St. Petersburg, Russia*, IFASD-2015-060.

[11] Gillebaart, E. and De Breuker, R. (2015). Reduced-order modeling of continuous-time state-space unsteady aerodynamics. In *53rd AIAA Aerospace Sciences Meeting*.

[12] Benner, P., Gugercin, S., and Willcox, K. (2015). A survey of projection-based model reduction methods for parametric dynamical systems. *SIAM Review*, 57(4), 483–531. ISSN 0036-1445. doi:10.1137/130932715.

[13] Amsallem, D. and Farhat, C. (2011). An online method for interpolating linear parametric reduced-order models. *SIAM Journal on Scientific Computing*, 33(5), 2169–2198.

[14] Lieu, T., Farhat, C., and Lesoinne, M. (2006). Reduced-order fluid/structure modeling of a complete aircraft configuration. *Computer methods in applied mechanics and engineering*, 195(41), 5730–5742.

[15] Schmit, R. and Glauser, M. (2003). Improvements in low dimensional tools for flow-structure interaction problems: using global pod. In *APS Division of Fluid Dynamics Meeting Abstracts*, vol. 1.

[16] Vassberg, J. C., DeHaan, M. A., Rivers, S. M., et al. (2008). Development of a common research model for applied cfd validation studies. In *26th AIAA Applied Aerodynamics Conference, Honolulu, Hawaii*.

[17] European Aviation Safety Agency (15 July 2015). *Certification Specifications and Acceptable Means of Compliance for Large Aeroplanes CS-25*. Amendment 17.

[18] Kassapoglou, C. (2013). *Design and analysis of composite structures: with applications to aerospace structures*. John Wiley & Sons.

[19] Hammer, V. B., Bendsøe, M., Lipton, R., et al. (1997). Parametrization in laminate design for optimal compliance. *International Journal of Solids and Structures*, 34(4), 415–434.

[20] Raju, G., Wu, Z., and Weaver, P. (2014). On further developments of feasible region of lamination parameters for symmetric composite laminates. In *55th AIAA/ASMe/ASCE/AHS/SC Structures, Structural Dynamics, and Materials Conference*. p. 1374.

[21] Wu, Z., Raju, G., and Weaver, P. M. (2015). Framework for the buckling optimization of variable-angle tow composite plates. *AIAA Journal*, 53(12), 3788–3804.

[22] Khani, A., IJsselmuiden, S. T., Abdalla, M. M., et al. (2011). Design of variable stiffness panels for maximum strength using lamination parameters. *Composites Part B: Engineering*, 42(3), 546–552.

[23] Dillinger, J., Klimmek, T., Abdalla, M. M., et al. (2013). Stiffness optimization of composite wings with aeroelastic constraints. *Journal of Aircraft*, 50(4), 1159–1168.

[24] Svanberg, K. (2002). A class of globally convergent optimization methods based on conservative convex separable approximations. *SIAM journal on optimization*, 12(2), 555–573.

COPYRIGHT STATEMENT